Multiple Target Tracking and Filtering using Bayesian Diabatic Quantum Annealing

Timothy M. McCormick, Zipporah Klain, Ian Herbert,
Anthony M. Charles, R. Blair Angle, Bryan R. Osborn, Roy L. Streit
Metron, Inc.
1818 Library St., Suite 600
Reston, VA 20190
{McCormickT, Klain, Herbert, CharlesA, Angle, Osborn, Streit}@metsci.com

Abstract—**In this paper, we present a hybrid quantum/classical algorithm to solve an NP-hard combinatorial problem called the multiple target data association (MTDA) and tracking problem. We use diabatic quantum annealing (DQA) to enumerate the low energy, or high probability, feasible assignments, and we use a classical computer to find the Bayesian expected mean track estimate by summing over these assignments. We demonstrate our hybrid quantum/classical approach on a simple example. This may be the first demonstration of a Bayesian hybrid quantum-classical multiple target tracking filter. We contrast our DQA method with the adiabatic quantum computing (AQC) approach to MTDA. We give a theoretical overview of DQA and characterize some of the technical limitations of using quantum annealers in this novel diabatic modality.**

TABLE OF CONTENTS

1. INTRODUCTION

To compute the (Bayesian) posterior distribution in multi-target tracking and data association (MTDA) problems, we need to evaluate a probabilistic sum, each term of which is conditioned on exactly one feasible assignment of measurements to targets. Enumerating the feasible assignments is an NP-hard combinatorial problem.

The fundamental quantity of interest in Bayesian inference is the posterior distribution. Point estimates, when needed, are "extracted" from the posterior by Bayesian decision theoretic methods (e.g., minimum risk). Two common point estimators are the MAP (maximum a posteriori) and the mean of the posterior distribution, both of which are used in tracking.

Adiabatic quantum computing (AQC) methods are used in [1], [4], [5] to find the optimal assignment. Conditioned on this assignment, target tracks are computed by classical

methods. In contrast, Bayesian methods do not select the best assignment, but instead sum over all the assignments. Thus, Bayesian methods are better suited to real world problems that often have high false alarm rates and low target detection probabilities.

This paper shows that diabatic quantum annealers (DQA) can be used to compute the Bayesian mean target state estimator. DQA finds a collection of low-energy configurations that are near but not necessarily in the ground state. Thus, in sharp contrast to AQC, DQA deliberately violates the adiabatic condition in order to anneal to a set of low-energy configurations. The DQA-generated collection of low-energy states is then passed to a classical computer to compute the mean state estimator.

Finding the low-energy configurations is a high computational complexity problem on a classical computer, but computing the mean state given the low-energy configurations is not. This is consistent with the over-arching strategy of exploiting QC methods to solve the NP-hard part(s) of a problem, which are often combinatorial, and then coupling the QC output with a classical computer to calculate the target tracks.

Section 2 deals with the mathematical details of the JPDA tracking filter. Section 3 discusses the transformation of the MTDA problem into an Ising model suitable for calculating on a QC such as D-Wave's 2000Q. Section 4 discusses using DQA to find low-energy non-ground states. Section 5 presents results. Section 6 gives results of using DQA to find feasible configurations, i.e., assignments. To our knowledge, this is the first demonstration of a Bayesian hybrid quantum-classical multiple target tracking filter. Section 7 summarizes our findings about the utility of DQA for Bayesian inference.

2. DATA ASSOCIATION AND TRACKING

The joint probabilistic data association (JPDA) filter [6] is a classical Bayesian target filter that estimates the joint posterior PDF for a known number of targets, N, by fusing multiple target-measurement assignment hypotheses in a principled manner. The JPDA filter is NP-hard because the number of assignments grows rapidly with problem size.

In the JPDA model, targets are assumed to be independent of one another and causally independent of the measurement process. At each scan k, a sensor produces a set of $M_k \geq 0$ point measurements, each of which is either target-induced or the result of an independent clutter (false alarm) process. A given target generates at most one sensor measurement per scan, and any given measurement is assigned to exactly one of the targets or to the clutter process. All point measurements

are superposed in a common measurement space $\mathcal{Y}$.

The JPDA model is inherently flexible and is amenable to particle filter (sequential Monte Carlo) methods. As the primary focus of this paper is target-measurement assignments, the JPDA model employed will adopt all of the original/standard JPDA assumptions. These simplifying assumptions, described below for a specific scenario, allow for an analytical solution of the posterior PDF, namely, a multivariate Gaussian.

In the tracking example in this paper, units of length are in meters, and time units are in seconds. Scans occur at one second intervals, beginning at time $t_1 = 1$; i.e., $\Delta t = 1$. The k-th scan occurs at time $t_k = k$ (the scan time is defined as the end time of the scan interval). There are $N = 4$ targets, with identical state spaces: $\mathcal{X}^n \equiv \mathcal{X} \subset \mathbb{R}^4$, $n = 1, \ldots, N$. The state vector for target n at scan k comprises two spatial components, x and y, and two velocity components, $\dot{x}$ and $\dot{y}$, and is denoted $x_k^n = (x_k^n, \dot{x}_k^n, y_k^n, \dot{y}_k^n)$.

At the reference time, $t_0 = 0$, no measurements are available and target n is assumed to have prior PDF $\mu_0^n(x_0^n) = \mathcal{N}(x_0^n; \hat{x}_{0|0}^n, P_{0|0}^n)$, where $\mathcal{N}(x; \mu, \Sigma)$ represents the PDF of a multivariate Gaussian with mean vector μ and covariance matrix Σ evaluated at x. Due to the assumption of target independence, the joint prior PDF for all target states is the product over n of the marginals $\mu_0(x_0^n)$, that is,

$$p_0(x_0^1, \ldots, x_0^N) = \prod_{n=1}^N \mu_0^n(x_0^n) = \prod_{n=1}^N \mathcal{N}\left(x_0^n; \hat{x}_{0|0}^n, P_{0|0}^n\right). \tag{1}$$

As will be seen, the JPDA filter imposes this factored form at each step k of the recursion. This is an approximation, and it ensures the posterior distribution has the exact same mathematical form as the prior distribution. In other words, the approximation closes the Bayesian recursion.

Targets move according to the linear-Gaussian motion model

$$p(x_k^n \mid x_{k-1}^n) = \mathcal{N}\left(x_k^n; F x_{k-1}^n, Q_{\text{proc}}\right), \tag{2}$$

where the process (motion) matrix F and the process noise covariance matrix Q_{proc} are given by

$$F = \begin{pmatrix} 1 & \Delta t & 0 & 0 \\ 0 & 1 & 0 & 0 \\ 0 & 0 & 1 & \Delta t \\ 0 & 0 & 0 & 1 \end{pmatrix}, \quad Q_{\text{proc}} = \sigma_p^2 \begin{pmatrix} \frac{\Delta t^3}{3} & \frac{\Delta t^2}{2} & 0 & 0 \\ \frac{\Delta t^2}{2} & \Delta t & 0 & 0 \\ 0 & 0 & \frac{\Delta t^3}{3} & \frac{\Delta t^2}{2} \\ 0 & 0 & \frac{\Delta t^2}{2} & \Delta t \end{pmatrix}.$$

We take $\sigma_p = 3$. These matrices are independent of scan index k.

At each scan, target n generates a sensor measurement with (constant) probability of detection $p_d = 0.9$. The (bounded) measurement space $\mathcal{Y} = [-600\text{m}, 600\text{m}] \times [-600\text{m}, 600\text{m}] \subset \mathbb{R}^2$ comprises the two spatial components x and y. Given a measurement $y = (x, y)$ induced by target n at scan k, the measurement likelihood has the following linear-Gaussian form:

$$p(y \mid x_k^n) = \mathcal{N}(y; H x_k^n, R), \tag{3}$$

where the measurement matrix $H = \begin{pmatrix} 1 & 0 & 0 & 0 \\ 0 & 0 & 1 & 0 \end{pmatrix}$ extracts the

two spatial components of x_k^n, and $R = \sigma_M^2 \begin{pmatrix} 1 & 0 \\ 0 & 1 \end{pmatrix}$, $\sigma_M = 25 \text{ m}^2$, is the measurement covariance.

The clutter model employed is a homogeneous Poisson point process (PPP) with mean $\lambda = 1$. That is, at each scan the number, n_c, of clutter points is generated according to a Poisson probability mass function (PMF) with mean λ. If $n_c > 0$, the clutter points are then uniformly and independently distributed over the the entire measurement space (field of view) $\mathcal{Y}$, the area of which is denoted $|\text{FoV}| = 1.44 \times 10^6 \text{ m}^2$.

Let $y_k = \{y_k^1, \ldots, y_k^{M_k}\}$ be the measurement set at scan k. If the target-measurement assignment is known, then the exact Bayesian posterior distribution is obtained via N independent Kalman filter updates (see [6]) and is of the same form as the prior given in Eqn. (1), namely, the product of N independent Gaussians. However, since the assignments are unknown, the exact Bayesian posterior is a weighted sum over all feasible assignment matrices S (see Eqn. (7) in Ref. [4]), i.e., a (large) Gaussian mixture of the form

$$p_k(x_k^1, \ldots, x_k^N | y_k) = \sum_S \Pr_k\{S|y_k\} \prod_{n=1}^N p_k^n(x_k^n|S, y_k), \tag{4}$$

where $p_k^n(x_k^n|S, y_k)$ is the Kalman updated posterior Gaussian for target n under assignment S, and $\Pr_k\{S|y_k\}$ is the posterior probability of assignment S; see Sect. 6. To close the Bayesian recursion, the multitarget posterior PDF is approximated as the product of N independent Gaussians in the same form as (1). In JPDA, this is done by replacing each posterior marginal, which is a Gaussian mixture, with a single multivariate Gaussian with the same mean and covariance.

3. THE ISING MODEL FOR MTDA

Optimization Variables as Qubits

Following Refs. [1], [2], we may write each entry of the association matrix S_{ij} of Eqn. (7) in Ref. [4] as the state of a two-level quantum system $|\phi_{ij}\rangle \in \{|0\rangle, |1\rangle\}$. The presence or absence of an association is represented as one of the basis states of the two-dimensional complex Hilbert space given by

$$|0\rangle = \begin{pmatrix} 1 \\ 0 \end{pmatrix}, \quad |1\rangle = \begin{pmatrix} 0 \\ 1 \end{pmatrix}, \tag{5}$$

which are eigenvectors (with eigenvalues 1 and -1, respectively) of the Pauli matrix σ_3, which in this basis is given by $\sigma_3 = \begin{pmatrix} 1 & 0 \\ 0 & -1 \end{pmatrix}$. The full state for the system in Eqn. (7) in Ref. [4] is the Kronecker product

$$|\Phi_j\rangle = |\phi_{00}\rangle \otimes \cdots \otimes |\phi_{MN}\rangle, \tag{6}$$

where j is the integer corresponding to the binary string of association matrix entries:

$$j \longleftrightarrow (S_{00}, S_{01}, \ldots, S_{MN}). \tag{7}$$

In this way, all possible (feasible and infeasible) associations can be written as $D = 2^{(M+1)(N+1)}$ dimension quantum states formed from Kronecker products of σ_3 eigenstates.

Optimization Problems as Ising Models

Determining high-likelihood configurations of association variables is a manifestly classical problem. Valid configurations are given only by tensor products of Eqn. (5) and hence

the cost of a particular configuration of association variables can be written only in terms of powers of mutually commuting σ_3 operators. We restrict our discussion to configuration costs that are at most quadratic in the association variables such that all possible costs are given by eigenvalues of the Hamiltonian

$$H_P = \sum_{i,j=1}^{N_s} Q_{ij}\sigma_3^i\sigma_3^j + \sum_{i=1}^{N_s} q_i\sigma_3^i. \qquad (8)$$

In Eqn. (8), Q_{ij} captures interaction costs while q_i captures "biases" on all N_s individual variables. The operator σ_3^i is

$$\sigma_3^i = \underbrace{\sigma_0 \otimes \cdots \otimes \sigma_0}_{i-1 \text{ terms}} \otimes \sigma_3 \otimes \underbrace{\sigma_0 \otimes \cdots \otimes \sigma_0}_{N_s-i \text{ terms}}, \qquad (9)$$

where σ_0 is the 2×2 identity matrix.

The Hamiltonian in Eqn. (8) is that of an Ising model, and it can be thought of as a finite-dimensional matrix whose entries are energies in the quantum mechanical sense that correspond exactly with the cost of association in the optimization problem of interest. However, finding the equivalent optimal configurations exhaustively would require a number of trials that scales exponentially as 2^{N_s}. In the next section, we describe a quantum method to efficiently solve for low-cost configurations using a quantum annealer. In Sections 5 and 6 we describe precise forms of Q_{ij} and q_i for two related problems of interest.

4. DIABATIC QUANTUM ANNEALING

The Instantaneous Hamiltonian

In quantum annealing, the system at the instantaneous time t is governed by the Hamiltonian

$$H(t) = A(t)H_B + B(t)H_P, \quad t_0 \leq t \leq t_f, \qquad (10)$$

where $A(t)$ and $B(t)$ are real-valued time-dependent coefficients. The functional form of these coefficients comprise an *annealing schedule*. In the simplest case, which we refer to as *forward annealing*, $A(t)$ monotonically decreases to 0 and $B(t)$ monotonically increases to 1.

Throughout this work, we will only consider H_B of the form

$$H_B = -\sum_{i=1}^{N_s} \sigma_1^i, \qquad (11)$$

where, in analogy with Eqn. (9),

$$\sigma_1^i = \underbrace{\sigma_0 \otimes \cdots \otimes \sigma_0}_{i-1 \text{ terms}} \otimes \sigma_1 \otimes \underbrace{\sigma_0 \otimes \cdots \otimes \sigma_0}_{N_s-i \text{ terms}}. \qquad (12)$$

Here σ_1 is the Pauli matrix $\sigma_1 = \begin{pmatrix} 0 & 1 \\ 1 & 0 \end{pmatrix}$. Since σ_1 and σ_3 do not commute, it is clear that, in general, H_B and H_P do not commute. Therefore, $H(t)$ is not diagonal in the computational basis given by Eqn. (5), except when $A(t) = 0$. The off-diagonal elements induce transitions between configurations in the computational basis.

Time Evolution in Quantum Annealing

At $t = 0$, the system is prepared in an initial state that we denote $|\psi(0)\rangle$. During the course of the quantum annealing

process, physical parameters of the device are modified following an annealing schedule $\{A(t), B(t)\}$ such that at any point in time t the system evolves according to

$$|\psi(t)\rangle = U(t,0)|\psi(0)\rangle. \qquad (13)$$

The solution of this system of time-dependent ordinary differential equations is the quantum time-evolution operator $U(t,0)$. It is written

$$U(t,0) = \mathbb{T}\exp\left(-i\int_0^t dt'\, H(t')\right), \qquad (14)$$

where $H(t')$ is the quantum Hamiltonian and $\mathbb{T}\exp(\cdot)$ denotes the time-ordered exponential function which, expanded as a power series, is

$$\mathbb{T}\exp\left(-i\int_0^t dt'\, H(t')\right)$$
$$= \sum_{n=0}^{\infty}(-i)^n \int_0^t dt'_n \cdots \int_0^{t'_2} dt'_1\, H(t'_n)\cdots H(t'_1), \quad (15)$$

where $t > t_n > t_{n-1} > ... > t_1$. Only in the specific case when the Hamiltonian commutes at different times, i.e.,

$$\left[H(t_1), H(t_2)\right] = 0, \ \forall t_1, t_2, \qquad (16)$$

does the time-ordered exponential reduce to the more familiar form $U(t,0) = \exp\left(-i\int_0^t dt' H(t')\right)$.

Diabatic Transitions

We write the Hamiltonian in Eqn. (10) as $\mathcal{H}(s) \equiv H(st_f)$, where t_f is the final evolution time and $s \equiv t/t_f \in [0,1]$ is dimensionless. The paradigm of *adiabatic* quantum annealing is to begin in a known and simple-to-prepare state $|\psi_0(0)\rangle$, often taken to be the ground state of H_B, and evolve the system *slowly*. The evolution of the system with Hamiltonian (10) is adiabatic if the "energy gap" $|E_n(s) - E_m(s)|$ between any two instantaneous eigenstates of $\mathcal{H}(s)$ (with labels n and m) is sufficiently large compared to the rate of evolution [7]:

$$\frac{1}{t_f}\max_{s\in[0,1]} \frac{|\langle n(s)|\,\partial_s\mathcal{H}(s)\,|m(s)\rangle|}{|E_n(s) - E_m(s)|} \ll 1, \forall m \neq n. \quad (17)$$

Under this condition, the time evolution given by Eqn. (14) simplifies such that the system remains in the ground state at all times and thus $|\psi_0(t_f)\rangle$ is the ground state of H_P.

For the purposes of tracking and multi-target data association, the lowest cost "optimal" configuration (the ground state) may be a relatively low probability configuration due to a large number of other configurations that have slightly higher energies. (This abundance of low-energy but non-ground state configurations is related to the fact that the difficulty of the MTDA problem increases rapidly as function of the number of targets and the false alarm density.) The Bayesian paradigm addresses this difficulty head-on by asserting, boldly, that the fundamental quantity of interest is the posterior distribution. Point estimators are ancillary statistics derived from the posterior.

Target state estimates used in this paper are expected values of the posterior distributions. The expectations are estimated by summing over the feasible configurations, weighted by their likelihoods. We use DQA to find the "low-energy" states to use in the Bayesian filter. Consequently, for our purposes, it is actually desirable to violate the condition in Eqn. (17) in order to anneal to states which are higher in energy than the ground state.
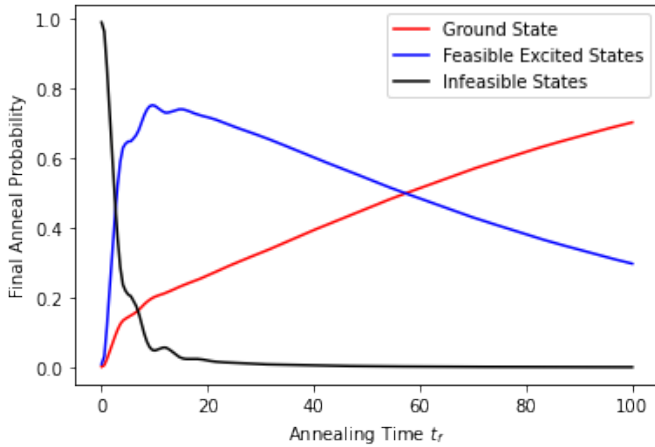
Figure 1: Final annealing probabilities for biased $k = 3$ rooks problem obtained by classical numeric computation QuTiP. Units of anneal time are inverse energy. A broad interval is observed for t_f where the feasible excited states are annealed to.

Annealing to Excited States

When a violation of adiabaticity occurs, quantum transitions are induced from the ground state into excited states. In practice, since any annealing on a physical device must occur with a finite t_f, these transitions occur with relatively high probability. This was noted in previous work on the application of quantum annealing to the MTDA problem [4]. Too high an annealing rate, however, leads to a sequence of scatterings to high-energy states throughout the annealing process. Consequently, for sufficiently small anneal times t_f, excited states not relevant to the tracking and association process (due to their infeasibility) are populated with high probability. Hence, we seek an intermediate range of values for t_f such that only the ground state and low-energy feasible excited states are populated with high probability.

The eigenstates of the final Hamiltonian H_P form a complete basis which we may use to expand any arbitrary state. We may thus expand the final state after annealing

$$|\psi(t)\rangle = \sum_{j=0}^{D-1} c_j(t) |\Phi_j\rangle, \quad (18)$$

where $D = 2^{N_s}$ and $|\Phi_j\rangle$ for our problems of interest are given by Eqn. (6). The transition probability amplitudes from the initial state $|\psi(0)\rangle$ to one of the states in the computational product space $|\Phi_j\rangle$ (after an annealing time t_f) are given by

$$\langle\Phi_j| U(t_f, 0) |\psi(0)\rangle = \langle\Phi_j|\psi(t_f)\rangle. \quad (19)$$

From orthogonality of the eigenstates, the probability of annealing from $|\psi(0)\rangle$ to a state $|\Phi_j\rangle$ is given by

$$p_j = |\langle\Phi_j|\psi(t_f)\rangle|^2 = |c_j(t_f)|^2. \quad (20)$$

A direct calculation of the transition amplitudes through solution of Eqns. (13-14) depends on the precise form of the initial state $|\psi(0)\rangle$, the final problem Hamiltonian H_P, and the anneal schedule $\{A(t), B(t)\}$. Obtaining a closed form solution is impossible in all but the simplest cases. However, for small system sizes, we can numerically calculate the spectrum exactly by diagonalizing the Hamiltonian on

a classical computer. Using the exact eigenspectrum, we numerically calculate the time evolution of the dynamics of a simple system using the GKSL master equation [8], [9], [10], [11] in QuTiP [12], [13].

In Fig. 1 we show annealed occupation probabilities for the ground state, the feasible excited states, and the infeasible excited states as a function of the final anneal time t_f for a biased $k = 3$ rooks problem. We take the parameters of the final problem Hamiltonian H_P to be given by Eqns. (24) and (30). We take the bias term to be drawn from a normal distribution $q_b \sim \mathcal{N}(0, 0.01)$. We see that for very small anneal times, the final annealed states are dominated by higher-energy infeasible states (black curve). Conversely, for very large values of t_f, the ground state probability is largest, as predicted by Eqn. (17). For an intermediate range of t_f, we see that the final annealed states comprise both the ground state as well as feasible excited states while the probability of annealing to one of the infeasible states becomes small, despite their large number $(2^{k^2} - k!)$.

5. DIABATIC QUANTUM ANNEALING FOR FEASIBLE CONFIGURATIONS

In the previous section, by solving the GKSL master equation we showed that we theoretically expect diabatic quantum annealing to obtain feasible, low-energy states corresponding to low-cost combinatorial assignments in the k-rooks problem. In this section, we validate this theoretical prediction using a D-Wave 2000Q QPU and study the how the fraction of feasible states that we obtain for a given number of quantum anneals depends on the system size. We also show that the performance of diabatic quantum annealing depends strongly on the details of the anneal schedule itself.

The Biased k-rooks Hamiltonian

In the absence of false alarms and missed detections, the MTDA problem can be modeled as a k-rooks problem [3]. In the k-rooks problem, a $k \times k$ chessboard is populated with k mutually non-threatening rooks. We wish to represent the Ising form H_P of the k-rooks problem in order to energetically impose the constraint of one rook per column and row. Following the notation of [3] and [4], we define the following

$$\mathbf{1}(k) \equiv k \times 1 \text{ column vector of ones}$$
$$= (1 \quad 1 \quad 1 \quad \cdots \quad 1)^T \quad (21)$$
$$I(k) \equiv k \times k \text{ identity matrix} \quad (22)$$
$$J(k) \equiv \mathbf{1}(k)\mathbf{1}(k)^T - I(k)$$
$$= k \times k \text{ matrix of ones, with zero diagonal}$$
$$= \begin{pmatrix} 0 & 1 & 1 & \cdots & 1 \\ 1 & 0 & 1 & \cdots & 1 \\ 1 & 1 & 0 & \cdots & 1 \\ \vdots & \vdots & \vdots & \ddots & \vdots \\ 1 & 1 & 1 & \cdots & 0 \end{pmatrix}. \quad (23)$$

The matrix of the quadratic term in the Ising Hamiltonian in Eqn. (8) for the k-rooks problem is given by

$$Q_{\text{kR}} = W_r + W_c, \quad (24)$$

and the linear term is given by

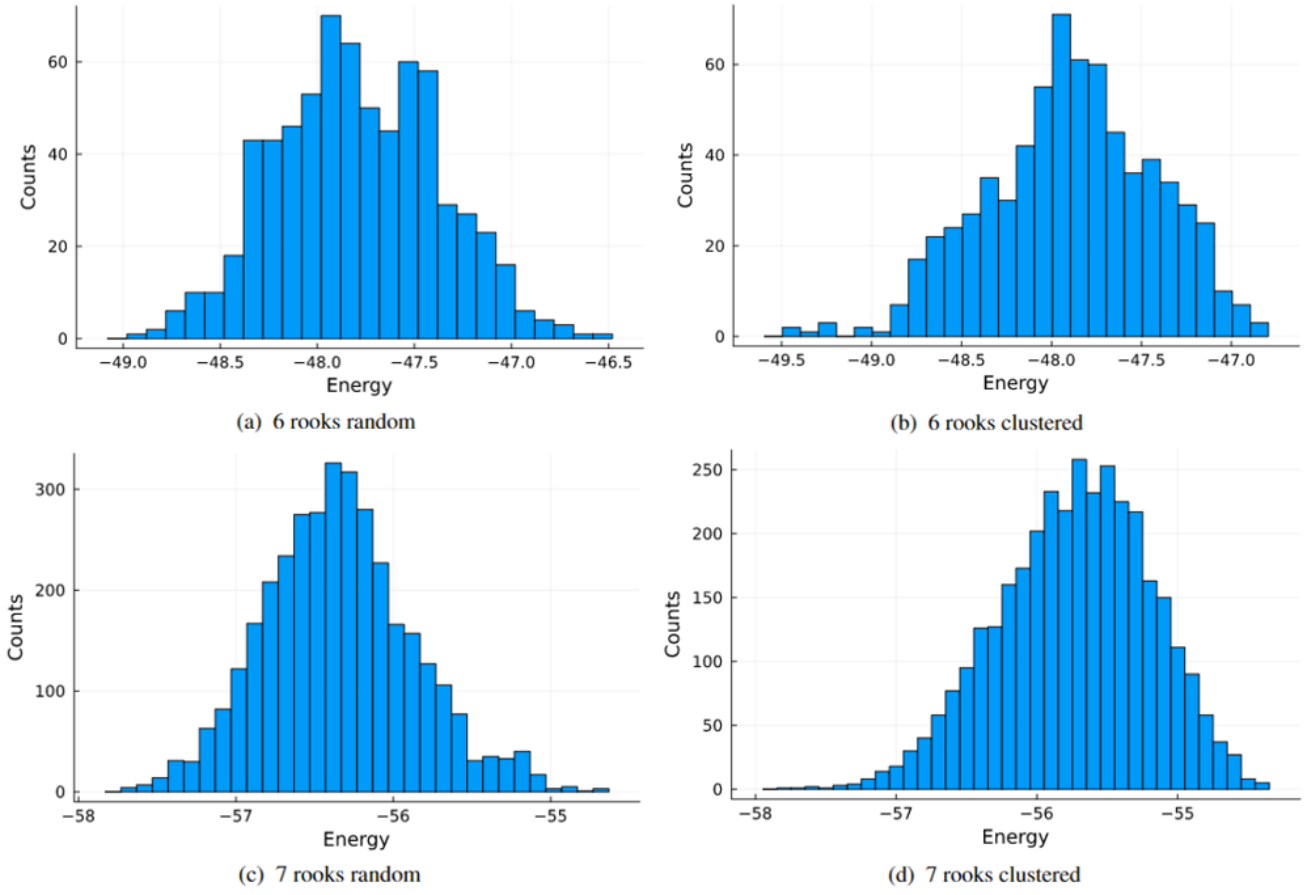$$q_{\text{kR}} = \theta_r + \theta_c. \quad (25)$$

4

(a) 6 rooks random

(b) 6 rooks clustered

(c) 7 rooks random

(d) 7 rooks clustered

Figure 2: Unique feasible states found in 10^6 shots on D-Wave 2000Q for different k-rooks variations

The $k^2 \times k^2$ matrix

$$W_r \equiv I(k) \otimes J(k) \qquad (26)$$

and the $k^2 \times 1$ column vector

$$\theta_r \equiv (2k - 4)\mathbf{1}(k^2) \qquad (27)$$

constrain the rows to have one rook each. Similarly,

$$W_c \equiv J(k) \otimes I(k) \qquad (28)$$

and

$$\theta_c \equiv (2k - 4)\mathbf{1}(k^2) \qquad (29)$$

constrain the columns to have one rook each.

The Ising Hamiltonian for the k-rooks problem described by Eqns. (24)-(25) has $k!$ degenerate ground states corresponding to the $k!$ different feasible configurations of rooks. Previous work [4] demonstrated that these ground states can be obtained by a quantum annealer. The high ground state degeneracy of the k-rooks Hamiltonian reflects the high degree of symmetry of the underlying problem.

This degeneracy can be broken by the addition of a bias to the linear term. We define

$$q_{kRB} = q_{kR} + q_b, \qquad (30)$$

where q_b is a $k^2 \times 1$ column vector whose elements correspond to costs for each space on the chess board (or equivalently to an on-site bias in the Ising Hamiltonian H_P). We find that the addition of this bias term leads to a structured low-energy manifold of feasible states.

Feasible configurations for the k-rooks problem

In this section, we obtain the low-energy costs and configurations of the k-rooks and MTDA systems using a D-Wave 2000Q QPU. For the k-rooks experiments we specify a chain strength of 8. To stimulate more rapid mixing to low-energy configurations, we use reverse annealing with an initial configuration of rooks along the diagonal and a pause-and-quench [14], [15] annealing schedule. Specifically, we anneal to the pause point at $s = 0.45$ in 5 μs, pause at that point for 93 μs, and then quench to the final Hamiltonian in 1 μs (for a total anneal time of 99 μs). Fig. 4 demonstrates the potential utility of reverse annealing and different pause points for a small number of shots (10^4). See the last paragraph of this section for further discussion.

In Fig. 2, we show the the distribution of unique feasible states that D-Wave finds in 10^6 shots for different variations of the k-rooks problem. These histograms show the density of annealed states. As the number of shots is increased, the probability of obtaining all feasible states empirically is found to approach unity (see Fig. 3). The counts in Fig. 2 correspond to the total unique feasible states found.
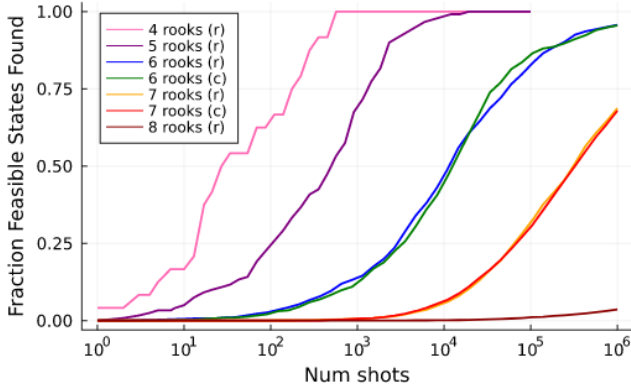
Figure 3: Unique feasible states accumulated over shots for different configurations of k-rooks (r = random bias, c = clustered)
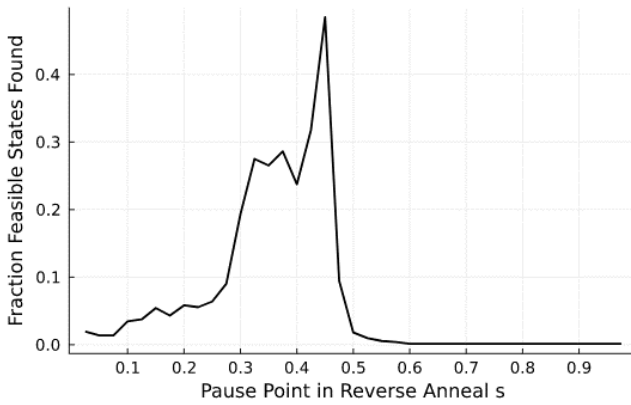

Figure 4: Dependence on anneal schedule of the number of unique feasible states found in 10^4 shots for $k = 6$ rooks and random Gaussian bias.

Generating a good solution to the MTDA problem relies on finding as many of the feasible states as possible, but the frequency with which each of those states occur in the returned shots is not relevant.

In Figs. 2 and 3, we call certain k-rooks variations "random" ("r") or "clustered" ("c"). This refers to the on-site bias (q_b in Eqn. 30) applied to each square of the kxk board. In the random variations, the bias is drawn from a Gaussian distribution $q_b \sim \mathcal{N}(0, 0.1)$ homogeneously across the entire board. For the clustered variations, the signs of the randomly drawn biases are adjusted so that certain blocks along the diagonal have considerably smaller bias (i.e., contribute lower energy) than squares outside those blocks. Since the k-rooks system is equivalent to the MTDA problem with no misses or false alarms, this biased variation models a system where there are several clusters of targets and measurements which are harder to disambiguate than those from cluster to cluster. Feasible states that respect the block structure have lower energy than others, as reflected in the longer left-tail in the (b) and (d) histograms of Fig. 2. For the 6-rooks case the block sizes are $[1, 2, 3]$ and for the 7-rooks case they are $[2, 2, 3]$.

Fig. 3 shows, for the k-rooks problem, the fraction of feasible states found by quantum annealing as a function of the number of shots n_s for several different values of k

and for different bias variations. Although the proportion of total states that are feasible ($k!/2^{k^2}$) decreases rapidly as k increases, we find a remarkably large fraction of the possible feasible states: for 6-rooks, feasible states represent about 10^{-8} of the total states; for 7-rooks, the fraction drops to 9×10^{-12}. For both $k = 6$ and $k = 7$, the number of shots required for each bias variation (random vs. clustered) is very similar. Fig. 3 demonstrates for the k-rooks problem that DQA will find the feasible configurations even when they are like needles "lost" in a haystack of infeasible configurations.

As noted in the previous section, anneal parameter selection plays a critical role in obtaining as large a fraction of feasible states as possible. Using a reverse anneal pause-and-quench schedule, we found that the fraction of feasible states found depended strongly on the pause point (Fig. 4). Fig. 4 shows a slow rise as s increases to a sharp peak at $s = .45$ and an immediate fall-off afterwards in the fraction of feasible states found. In Fig. 4, we run anneals of 10,000 shots on a D-Wave 2000Q for a 6-rooks problem with random on-site bias, for every pause point in a grid of resolution 0.025.

6. MULTISTEP BAYESIAN RECURSION WITH QUANTUM ANNEALING

In this section the DQA algorithm discussed in Sec. 4 is used recursively to find feasible assignments. The DQA generated assignments are passed to a classical computer to find the track estimates via the JPDA recursion given in Sec. 2. The recursion is closed by passing the estimated tracks back to the DQA algorithm to find feasible assignments for the next scan. To our knowledge, this is the first demonstration of a Bayesian hybrid quantum-classical multiple target tracking filter.

The MTDA Hamiltonian

The Ising formulation of the MTDA problem comprises two different components in the problem Hamiltonian H_P. The first is a quadratic term that constrains the association of at most one target to each detection and at most one detection to each target. The second is a linear term that accounts for the cost of target-detection misassignment based on the negative log-likelihood. The linear term also contains the linear part of the association constraints, similar to Eqn. (25). Let $\gamma = \text{vec}(\mathbf{\Gamma})$ be as defined by Eqn. (9) from our previous work [4], and let $c > 0$ be given. Then the quadratic term that constrains the association of at most one target to each detection and at most one detection to each target leads to a modified form of the k-rooks cost matrix

$$Q_{\text{MTDA}} = c\,(W_r' + W_c'), \tag{31}$$

and the second term gives

$$q_{\text{MTDA}} = c\,(\theta_r' + \theta_c') + \gamma\,, \tag{32}$$

where W_r', W_c', θ_r', and θ_c' (defined below) are similar to the corresponding k-rooks constraints but are modified to allow for missed detections and false alarms. The cost constraint coefficient c sets the overall energy scale of the constraint terms; higher values correspond to more stringent enforcement of the feasibility constraints.

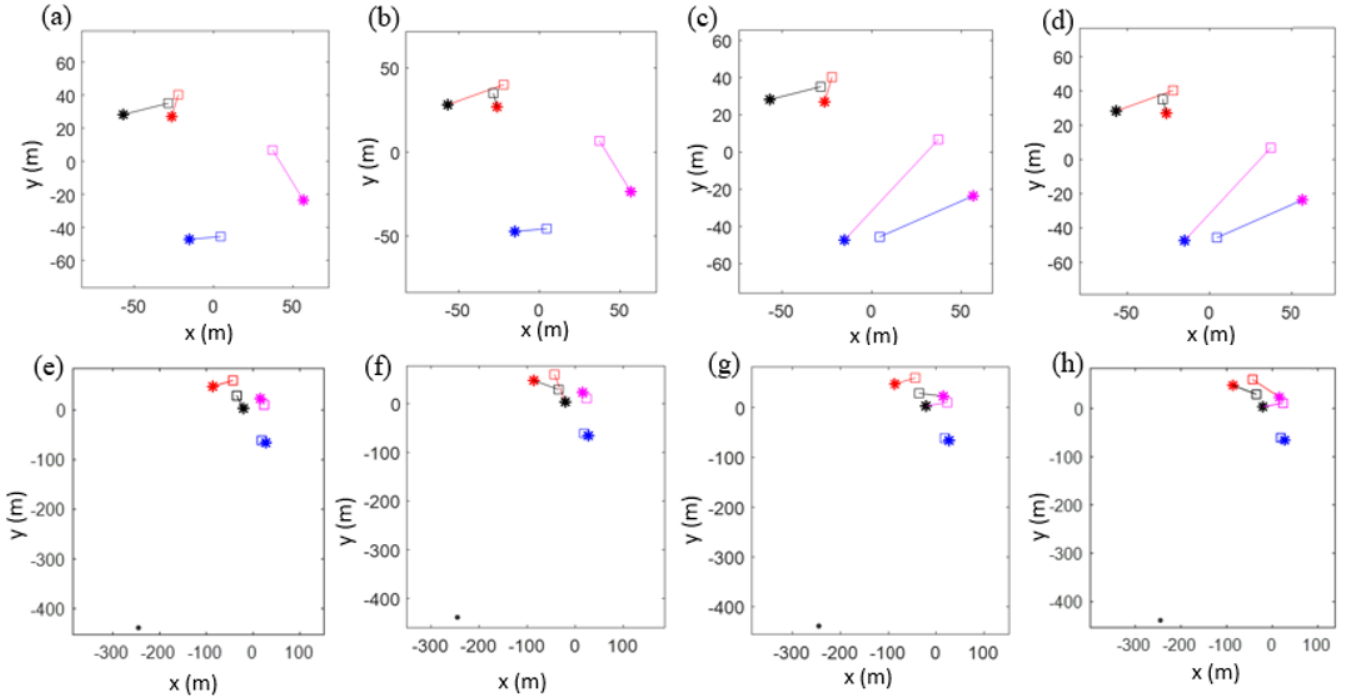With minor changes to Eqns. (21) and (22), we define the

Figure 5: Assignments from Multi-Step MTDA performed using DQA. □ = target, ∗ = measurement, ● = clutter. **(a)** Scan 1, Assignment 1, weight = 0.49596. **(b)** Scan 1, Assignment 2, weight = 0.42746. **(c)** Scan 1, Assignment 3, weight = 0.02806. **(d)** Scan 1, Assignment 4, weight = 0.02418. **(e)** Scan 2, Assignment 1, weight = 0.73170. **(f)** Scan 2, Assignment 2, weight = 0.12453. **(g)** Scan 2, Assignment 3, weight = 0.10950. **(h)** Scan 2, Assignment 4, weight = 0.02210.

following matrices:

$$\mathbf{1}_0(k) \equiv k \times 1 \text{ col vector of ones with zero in first entry}$$

$$= (0 \quad 1 \quad 1 \quad \cdots \quad 1)^T \tag{33}$$

$$I_0(k) \equiv k \times k \text{ identity matrix with zero in } (1,1) \text{ entry}$$

$$= \begin{pmatrix} 0 & 0 & 0 & \cdots & 0 \\ 0 & 1 & 0 & \cdots & 0 \\ 0 & 0 & 1 & \cdots & 0 \\ \vdots & \vdots & \vdots & \vdots & \vdots \\ 0 & 0 & 0 & \cdots & 1 \end{pmatrix} \tag{34}$$

For $N \geq 1$ targets and $M \geq 0$ measurements,

$$W_r' = I_0(M+1) \otimes J(N+1)$$
$$W_c' = J(M+1) \otimes I_0(N+1)$$
$$\theta_r' = (2N-2) \left[\mathbf{1}_0(M+1) \otimes \mathbf{1}(N+1) \right]$$
$$\theta_c' = (2M-2) \left[\mathbf{1}(M+1) \otimes \mathbf{1}_0(N+1) \right]. \tag{35}$$

We note that the MTDA constraint matrices in Eqn. (35) provide the correct expression of the matrices given in [1].

Results for Hybrid Quantum/Classical DQA/JPDA

We consider an $N = 4$ target tracking problem over multiple time scans. We take the PPP clutter model described in Sec. 2 with $\lambda = 1$ mean clutter measurements per scan. The prior object state for each target n is instantiated at reference time $t_1 = 1$ rather than $t_0 = 0$. The prior PDF is assumed to be normally distributed with mean $\hat{x}_{1|1}^n$ equal

to the corresponding ground truth at time t_1 and diagonal covariance $P_{1|1}^n = \text{diag}(25^2, 5^2, 25^2, 5^2)$; see Eqn. (1). At each time scan, a cost matrix Γ is derived from the posterior assignment $\Pr_k\{S|y_k\}$ in Eqn. (4) and converted into a linear bias γ in Eqn. (32). The related MTDA model (with $c = 2$) is then solved on a D-Wave 2000Q QPU using $n_s = 10^4$ shots. All feasible configurations (those satisfying Drummond's "at most one measurement per target per scan rule") that are returned by the DQA are then passed back to the classical JPDA tracker. They are then assigned weights according to $\Pr_k\{S|y_k\}$ and used to generate the prior PDF for the next scan.

In Fig. 5 we show the measurements and ground truth locations for the top four assignments (rank-ordered by their posterior weight) for two consecutive scans. Square icons show the ground truth locations, stars show the measurement locations for targets, and filled circles correspond to the locations of clutter measurements. Colored lines connecting ground truth and targets show the assignments returned by the DQA algorithm. The best scoring assignment for both scans assigns all of the targets and measurements properly.

In Fig. 6, we show tracks of all 4 targets over 19 consecutive time scans. Targets begin clustered tightly nearly the origin and move outward (ground truth shown as dashed lines). It is difficult to see in the figure, but the black and magenta targets cross roughly a quarter of the way through the simulation, making this a difficult tracking problem. Given the measurement errors, the JPDA tracker is not able to disambiguate these targets and assigns improper custody by the end of the scenario. The DQA generated assignments correctly reflect this reality in the data. Tracks on the blue and red targets are assigned properly.
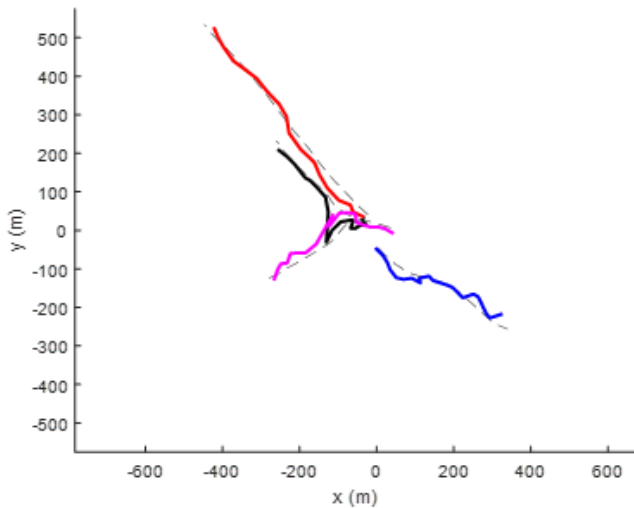
7

Figure 6: Hybrid DQA/classical track estimates for four targets by over 19 time steps. Target state estimates are the expected values obtained by summing over the DQA generated assignments. Targets are initialized near the origin and move outward. $Pd = 0.9$. False alarms are uniformly distributed and Poisson ($\lambda = 1$). (dashed lines = ground truth)

7. CONCLUDING REMARKS

In this paper we have demonstrated that diabatic quantum annealing can be used to efficiently explore the space of low-energy states for a wide range of Ising model Hamiltonians that are relevant for multi-target data association problems. These low-energy states correspond to nearly-optimal feasible assignments, and thus they can be summed over to compute Bayesian mean state estimators. Moreover, as seen in Fig. 6, this can yield accurate results for a non-trivial tracking problem, thereby concretely establishing the utility of our novel hybrid quantum/classical approach to a wide class of tracking problems.

One crucial point worth emphasizing is that the feasible low-energy states comprise only a tiny fraction of the full state space in the models explored in this work. In particular, for the k-rooks problem with $k \geq 6$, fewer than one in every 10^8 states represent feasible data associations, which makes classical approaches for finding such associations prohibitively expensive. Our DQA-based approach, however, yields almost all of these feasible associations for the $k = 6$ and $k = 7$ problems. Our approach to DQA-based feasible state identification will naturally extend to other models relevant for tracking problems, and we look forward to exploring these possibilities in upcoming work.

The efficiency of using DQA to find feasible states hinges on the selection of annealing schedules and annealing times that break adiabaticity "softly" enough to avoid annealing to high-energy states. As such, it would be worthwhile to develop a systematic and rigorous approach for determining how best to select the annealing parameters for any given MTDA problem. This can be done via a path integral Monte Carlo approach, wherein the full quantum time evolution of the Ising model is simulated by doing classical annealing on a large number of "replica" copies of the original model [16]. We leave such an analysis to future work.

REFERENCES

[1] F. Govaers, V. Stooß, M. Ulmke, "Adiabatic Quantum Computing for Solving the Multi-Target Data Association Problem," IEEE International Conf. on Multisensor Fusion and Integration (MFI), Karlsruhe, Germany, Sept. 23-25, 2021.

[2] V. Stooß, M. Ulmke, and F. Govaers, "Adiabatic Quantum Computing for Solving the Weapon Target Assignment Problem," arXiv: Quantum Physics, 2021. [Online]. Available: https://arxiv.org/abs/2105.02011

[3] C. Bauckhage, R. Sanchez, and R. Sifa, "Problem solving with Hopfield networks and adiabatic quantum computing," International Joint Conf. on Neural Networks (IJCNN), Glasgow, United Kingdom, July 14-24, 2020.

[4] T. M. McCormick, B. R. Osborn, R. B. Angle, and R. Streit, "Implementation of a Multiple Target Tracking Filter on an Adiabatic Quantum Computer," arXiv: Quantum Physics, 2021. [Online] Available: https://arxiv.org/abs/2110.08346

[5] J.-N. Zaech, A. Liniger, M. Danelljan, D. Dai, and L. Gool, "Adiabatic quantum computing for multi object tracking", Comp. Vis. and Pat. Rec., CVPR 2022, New Orleans, 19-24 June 2022.

[6] Y. Bar-Shalom and X.-R. Li, *Estimation and Tracking – Principles, Techniques, and Software*, YBS Publishing, Storrs, CT, USA, 1995.

[7] M. H. S. Amin, "Consistency of the Adiabatic Theorem," Phys. Rev. Lett., vol. 102, 2009. [Online]. Available: https://doi.org/10.1103/PhysRevLett.102.220401

[8] D. Manzanon, "A short introduction to the Lindblad master equation," AIP Advances 10, 025106, 2020. [Online]. Available: https://doi.org/10.1063/1.5115323

[9] S. Weinberg, "Quantum mechanics without state vectors," Phys. Rev. A, 90, 042102, 2014. [Online]. Available: https://doi.org/10.1103/PhysRevA.90.042102

[10] V. Gorini, A. Kossakowski, E. C. G. Sudarshan, "Completely positive dynamical semigroups of N-level systems," J. Math. Phys. 17, 5 821, 1976. [Online]. Available: doi:10.1063/1.522979

[11] G. Lindblad, "On the generators of quantum dynamical semigroups". Commun. Math. Phys. 48, 2 119, 1976. [Online]. Available: doi:10.1007/BF01608499.

[12] J. R. Johansson, P. D. Nation, and F. Nori, "QuTiP: An open-source Python framework for the dynamics of open quantum systems.", Comp. Phys. Comm. 183, 1760–1772, 2012. [Online]. Available: https://doi.org/10.1016/j.cpc.2012.02.021

[13] J. R. Johansson, P. D. Nation, and F. Noriac, "QuTiP 2: A Python framework for the dynamics of open quantum systems," Comp. Phys. Comm. 184, 1234, 2013. [Online]. Available: https://doi.org/10.1016/j.cpc.2012.11.019

[14] "Annealing Implementation and Controls," The D-Wave Company, 2020.

[15] "Reverse Quantum Annealing for Local Refinement of Solutions," The D-Wave Company, 2017.

[16] Yazhen Wang. Shang Wu. Jian Zou, "Quantum Annealing with Markov Chain Monte Carlo Simulations and D-Wave Quantum Computers," Statist. Sci. 31 (3) 362 - 398, August 2016. [Online]. Available: https://doi.org/10.1214/16-STS560

BIOGRAPHY

Timothy M. McCormick received his B.S. in physics from University of Delaware and his Ph.D. in theoretical physics from the Ohio State University, where his research focused on thermoelectric transport and electronic structure of topological semimetals. He is a research scientist at Metron Inc., where his work lies at the intersection of physics, statistics, and computation. His current interests include underwater acoustics, compressed sensing, multi-agent reinforcement learning, and quantum computation.

Zipporah Klain received a B.S. in Computer Science and a B.A. in Sociology from the University of Chicago in 2021. While there, her research spanned several domains, including effective quantum-computing education for all levels of students with the EPiQC and CANON labs. She is currently a software engineer at Metron, Inc., working on research and production projects focused on tracking, automated mission planning and optimization, and applications of quantum computing.

Ian Herbert received a B.S. in Mathematics and a B.A. in Russian from Tulane University, and a Ph.D. in Logic and the Methodology of Science from UC Berkeley. He is a research scientist in the Advanced Data Analytics division at Metron, Inc., where his work focuses on AI/ML, particularly adversarial-input attacks to ML systems and defenses against them. His current interests include Gaussian Processes, Graph Convolutional Networks, and anomaly detection.

Anthony M. Charles received a B.S. in physics and a B.A. in mathematics from the University of Virginia and a Ph.D. in theoretical physics from the University of Michigan, where his research focused on quantum aspects of black holes in string theory. He is currently a software engineer at Metron, Inc., where he works on research and development across a wide range of topics in physics and mathematics, including particle filtering and sequential Monte Carlo methods, optimal control theory, and quantum computing.

Bryan R. Osborn received B.S. degrees in Physics and Mathematics in 2001 and an M.S. in Applied Mathematics and Scientific Computation in 2004 from the University of Maryland, College Park. He is currently a Senior Research Scientist at Metron, Inc. where he leads development and application of tracking algorithms in a variety of contexts. His interests include distributed sensing systems, high-performance computing, and interactive visualization.

R. Blair Angle received his Ph.D. in mathematics from the University of California, San Diego, and is currently a senior research scientist at Metron, Inc. His current work involves multi-target tracking, data fusion, analytic combinatorics, and their interplay. He recently co-authored the book Analytic Combinatorics for Multiple Object Tracking, Springer, 2021.

Roy L. Streit joined Metron in 2005. His interests include multi-target tracking, multi-sensor data fusion, signal processing, medical imaging, and quantum computing. His recent work involves applications of analytic combinatorics to multi-target tracking, natural language processing, and subgraph matching in high level fusion. He is a Life Fellow of the IEEE. He co-authored Analytic Combinatorics for Multiple Object Tracking, Springer, 2021, and Bayesian Multiple Target Tracking, Second Edition, Artech, 2014. He is also the author of Poisson Point Processes: Imaging, Tracking, and Sensing, Springer, 2010. Before 2005, he was in Senior Executive Service at Naval Undersea Warfare Center, Newport, RI.